Distinct Transport Selectivity of Two Structural Subclasses of the Nodulin-like Intrinsic Protein Family of Plant Aquaglyceroporin Channels†

Ian S. Wallace and Daniel M. Roberts*

Department of Biochemistry and Cellular and Molecular Biology, The University of Tennessee, Knoxville, Tennessee 37996-0840

Received June 21, 2005; Revised Manuscript Received October 3, 2005

ABSTRACT: Major intrinsic proteins (MIPs) are a diverse class of integral membrane proteins that facilitate the transport of water and some small solutes across cellular membranes. X-ray structures of MIPs indicate that a tetrad of residues (the ar/R region) form a narrow pore constriction that constitutes the selectivity filter. In comparison with mammalian and microbial species, plants have a greater number and diversity of MIPs with greater than 30 genes encoding four phylogenetic subfamilies with eight different classes of ar/R sequences. The nodulin 26-like intrinsic protein (NIP) subfamily in *Arabidopsis* can be subdivided into two ar/R subgroups: the NIP subgroup I, which resembles the archetype of the family, soybean nodulin 26, and the NIP subgroup II, which is represented by the *Arabidopsis* protein AtNIP6;1. These two NIPs differ principally by the substitution of a conserved alanine (NIP subgroup II) for a conserved tryptophan (NIP subgroup I) in the helix 2 position (H2) of the ar/R filter. A comparison of the water and solute tranport properties of the two proteins was performed by expression in *Xenopus laevis* oocytes. Nodulin 26 is an aquaglyceroporin with a modest osmotic water permeability (P_f) and the ability to transport uncharged solutes such as glycerol and formamide. In constrast, AtNIP6;1 showed no measurable water permeability but transported glycerol, formamide, as well as larger solutes that were impermeable to nodulin 26. By site-directed mutagenesis, we show that the H2 position is the crucial determinant that confers these transport behaviors. A comparison of the NIPs and tonoplast-intrinsic proteins (TIP) shows that the H2 residue can predict the transport profile for water and glycerol with histidine found in TIP-like aquaporins, tryptophan found in aquaglyceroporins (NIP I), and alanine found in water-impermeable glyceroporins (AtNIP6;1).

Major intrinsic proteins (MIPs)[1] are an ancient family of integral membrane proteins that mediate the bi-directional flux of water (aquaporins) and uncharged small solutes such as glycerol (glyceroporins) across cellular membranes. MIPs are present in almost all organisms and are especially prevalent in plants with 35 full-length genes in the *Arabidopsis thaliana* genome (*1*, *2*) that can be subdivided into four phylogenetic subfamilies: the plasma membrane intrinsic proteins (PIPs), tonoplast intrinsic membrane proteins (TIPs), nodulin 26-like intrinsic proteins (NIPs), and small basic intrinsic proteins (SIPs). MIPs have been implicated in various physiological processes in plants such as cell elongation (*3*), adaptation and recovery from water deficit (*4*), anoxic stress (*5*), as well as many other phenomena that require rapid facilitated transport of water (reviewed in refs *6* and *7*).

The high-resolution X-ray structures of several members of the MIP family (*8*−*10*) have provided a wealth of information on the structure and function of these proteins at the atomic level. These structures reveal that the MIP family has a highly conserved "hourglass" fold (*11*), with six membrane-spanning α helices separated by five loop regions (loops A−E). Loops B and E contain symmetrically opposed, conserved Asn-Pro-Ala (NPA) motifs that form two short helices, which fold inward to form a seventh pseudo-transmembrane helix that interacts with the other transmembrane helices to form the pore of the protein (*8*−*10*).

The pore is characterized by two regions of constriction that determine transport selectivity and mediate the exclusion of ions including protons. The first (the NPA region) is formed by the close apposition of the asparagines of the two NPA motifs at the center of the pore. These asparagine residues form hydrogen-bond contacts with transported water and solute molecules and are proposed to block proton transport by interrupting the hydrogen-bonding network of the water chains by dipole reorientation of transported water (*12*, *13*). A second, narrower pore constriction is formed at the extracellular end of the pore from a tetrad of residues

† Supported by the National Science Foundation Grant MCB-0237219, National Institutes of Health Grant RR018470-01, as well as an National Science Foundation Graduate Research Fellowship to I.S.W.

* To whom correspondence should be addressed: Department of Biochemistry and Cellular and Molecular Biology, The University of Tennessee, Knoxville, TN. Telephone: 1-865-974-4070. Fax: 1-865-974-6306. E-mail: drobert2@utk.edu.

[1] Abbreviations: MIP, major intrinsic protein; PIP, plasma membrane intrinsic protein; TIP, tonoplast intrinsic protein; NIP, nodulin 26-like intrinsic protein; SIP, small basic intrinsic protein; H2, helix 2 position of the ar/R region; H5, helix 5 position of the ar/R region; LE_1, loop E 1 position of the ar/R region; LE_2, loop E 2 of position of the ar/R region; NPA, asparagine−proline−alanine motif; ar/R, aromatic/arginine region; P_f, osmotic water permeability coefficient; p_f, unitary water permeability; $\Delta H^{\ddagger}$, enthalpy of the transition state; $\Delta S^{\ddagger}$, entropy of the transition state; E_a, activation energy; AQP1, aquaporin 1; CDPK, calcium-dependent protein kinase.

10.1021/bi0511888 CCC: $30.25
Published on Web 12/01/2005

from helix 2, helix 5, and loop E (*8*−*10*), and this region serves as the selectivity filter. This region has been referred to as the "aromatic-arginine" (ar/R) region (*14*) based on the presence of a conserved arginine residue in loop E and the high prevalence of aromatic residues at helix 2 of the ar/R region.

The ar/R region determines both the selectivity and transport rate of MIPs by serving as a size-exclusion barrier sterically blocking the transport of bulkier substrates as well as providing key hydrogen-bond and van der Waals contacts for transported solutes and/or water molecules (*8*, *9*). Analysis of the ar/R regions of animal and microbial MIPs show that they can be segregated into two structural and functional classes, characteristic of either water-specific aquaporins or glycerol-transporting glyceroporins and aquaglyceroporins (*15*, *16*). In contrast, analysis of the residues of the diverse family of plant MIPs suggest considerable divergence from this paradigm, with unique ar/R regions found that can be classified into eight structurally distinct subgroups among the four phylogentic subfamilies, suggesting a greater diversity in the transport function of plant MIPs compared to their animal and microbial counterparts (*17*).

Soybean nodulin 26, the archetype of the NIP subfamily, is the major intrinsic protein of the symbiosome membrane of nitrogen-fixing root nodules (*18*−*20*). Nodulin 26 is an aquaglyceroporin with a low intrinsic water-transport rate (*20*, *21*) and is subject to regulation through phosphorylation by a calcium-dependent protein kinase (CDPK) (*18*, *22*, *23*). An examination of the *Arabidopsis* NIP subfamily reveals that NIPs can be subdivided into two subgroups (NIP I or II) based on the residues that compose their ar/R regions (*17*). NIP subgroup I contains the majority of the *Arabidopsis* NIPs and resembles soybean nodulin 26 at the ar/R region. In this study, we have functionally analyzed *Arabidopsis* AtNIP6;1, a member of the previously functionally uncharacterized NIP subgroup II. The results show that the NIPs of subgroup II have unique water and solute permeabilities distinct from NIP subgroup I and that these differences in transport properties are linked to amino acid substitutions in the ar/R region of the pore.

MATERIALS AND METHODS

Molecular Biology Techniques. An N-terminal FLAG epitope tag was inserted into the pXβG-ev1 *Xenopus* expression vector (*24*) by combining the following oligonucleotides to form a cassette:

5′-GATCCGAATTCATGGACTACAAAGACGACG-
ACGACAAAA-3′

3′-GCTTAAGTACCTGATGTTTC TGCTGCTGCT
GTTTTCTAG-5

The cassette contains *Bam*HI and *Bgl*II cohesive ends and an *Eco*RI restriction site at the 5′ end followed by the coding sequence for the FLAG epitope (MDYKDDDDK). The oligonucleotides (240 ng/μL) were phosphorylated by T4 polynucleotide kinase (Fisher) at 37 °C for 30 min, followed by denaturation of the enzyme by incubation at 65 °C for 15 min. pXβG-ev1 was digested with *Bgl*II and was dephosphorylated with shrimp alkaline phosphatase (Promega). The phosphorylated FLAG epitope cassette was ligated into the vector using the Takara ligation kit version II (Takara) and was transformed into *Escherichia coli* DH5α. Positive clones were verified by automated sequencing using a Perkin−Elmer Applied Biosystems 373 DNA sequencer using the Prism dye terminator reaction at the University of Tennessee Molecular Biology Research Facility.

The cDNA for AtNIP6;1 was obtained from *Arabidopsis thaliana* Columbia ecotype by reverse transcriptase PCR. The total RNA was isolated from 6-week-old *Arabidopsis thaliana* as described previously (*25*). Total RNA (1 μg) from roots, leaves, flowers, and stems was reverse-transcribed into cDNA using MMLV reverse transcriptase (Fisher). The reactions were incubated at 42 °C for 50 min followed by 2 min at 80 °C to denature the polymerase.

The following synthetic oligonucleotide primers were used to amplify the AtNIP6;1 open-reading frame (ORF) with flanking *Bgl*II restriction sites from the cDNA sample:

NIP6;1 forward, 5′-GGAAGATCTATGGATCATGA-
GGAAATTCCATCCACG-3′

NIP6;1 reverse, 5′-GGAAGATCTTCATCTTCTGAA-
GCTCCTCCTCTCTTTGGG-3′

The NIP6;1 ORF was amplified using *ExT aq* (Takara) under the following PCR conditions: 5 min of initial denaturation at 94 °C followed by 30 cycles at 94 °C (30 s), 55 °C (30 s), 72 °C (75 s), and a final extension at 72 °C (7 min). The PCR product was resolved by electrophoresis on a 1% (w/v) low-melting agarose gel and was purified by using the QiaQuick gel-excision kit (Qiagen). Gel-purified DNA was inserted into the TOPO cloning vector (Invitrogen) by the protocol of the manufacturer. The insert was digested from the TOPO vector with *Bgl*II and ligated into pXβG-ev1 with or without the FLAG epitope using the Takara ligation kit version II (Takara).

Site-directed mutants of AtNIP6;1 were generated directly on the pXβG-ev1 construct by the Quickchange method (Stratagene) with the following primers:

A119W F,
5′-TGCGCCGCCTCGTGGGGTTTGGCGGTT-3′

A119W R,
5′-AACCGCCAAACCCCACGAGGCGGCGCA-3′

V252A F,
5′-TCGATGAACCCTGCAAGAACACTGGGT-3′

V252A R,
5′-ACCCAGTGTTCTTGCAGGGTTCATCGA-3′

AtNIP6;1 mutants were amplified with *Pfu* polymerase (Stratagene) using the following cycling conditions: an initial denaturation for 10 min at 94 °C, followed by 30 cycles at 94 °C (30 s), 60 °C (30 s), 72 °C (8 min), and a final extension at 72 °C for 7 min. The PCR products were digested with *Dpn*I enzyme and were transformed into *E. coli* DH5α. Mutations were verified by automated DNA sequencing as described above.

Oocyte Expression and Transport Measurements. Stage V and VI oocytes were surgically removed from adult female oocyte positive *Xenopus laevis* frogs (*Xenopus* express), defolliculated, and cultured as previously described (*20*, *21*).

Capped cRNA was produced from *Xba*I-linearized pXβG-ev1 plasmids by *in vitro* transcription by using the mMessage mMachine (Ambion) kit. Oocytes were injected with 46 ng of cRNA and incubated at 16 °C for 72 h in individual wells of a 96-well plate in oocyte media (96 mM NaCl, 2 mM KCl, 5 mM $MgCl_2$, 0.6 mM $CaCl_2$, 5 mM HEPES at pH 7.6, and 1000 units of penicillin−streptomycin, osomolarity = 220 mOsm/kg). Negative control (uninjected) oocytes were cultured under identical conditions for the same duration prior to assay.

The osmotic water permeability (P_f) was measured as described previously (*21*). Assays were carried out at 15° C and were initiated by placing oocytes into hypoosmotic media consisting of 30% oocyte media (60 mOsm/kg) and monitoring the change in cross-sectional area by video microscopy. The P_f was determined from the calculated change in oocyte volume [$d(V/V_0)/dt$] by using the following form of the osmotic water permeability equation:

$$P_f = \frac{(V_0/S_0)(d(V/V_0)/dt)}{(S_{real}/S_{sphere})V_w(osm_{in} - osm_{out})}$$

where V_0 is the initial oocyte volume, S_0 is the initial oocyte surface area, osm_{in} is the osmolarity in the oocyte, osm_{out} is the osmolarity of the media, V_w is the partial molar volume of water, S_{real} is the actual area of the oolemma, and S_{sphere} is the area calculated by assuming a sphere. S_{real}/S_{sphere} is taken as 9 for all measurements (*21*).

Nonradiolabeled solute uptake assays were performed by equilibrating oocytes in full-strength standard oocyte media and measuring the swelling rate at 15 °C by video microscopy upon placement in a solution that contained the standard oocyte media with the NaCl replaced by 200 mM of test solute. The rate is reported as $d(V/V_0)/dt$.

Radiolabeled glycerol uptake assays were performed as described previously (*26*). Briefly, oocytes were incubated in a glycerol assay buffer (200 mM glycerol, 60 μCi/mL [^{3}H]-glycerol, 2 mM KCl, 5 mM $MgCl_2$, 0.6 mM $CaCl_2$, and 5 mM HEPES−NaOH at pH 7.6) for 10 min at 25 °C. Urea uptake assays were performed in a similar manner, except that an assay buffer consisting of 200 mM urea, 30 μCi/mL [^{14}C]-urea, 2 mM KCl, 5 mM $MgCl_2$, 0.6 mM $CaCl_2$, and 5 mM HEPES−NaOH at pH 7.6 was used. Oocytes were washed with 20 mL of ice-cold assay buffer without the isotope and were lysed in 300 μL of 10% (v/v) sodium dodecyl sulfate. A total of 10 mL of aqueous scintillation fluid was added, and the isotope uptake was quantified with a Beckman LS 3801 scintillation counter. Thermodynamic parameters describing the transition state of water transport through the nodulin 26 and AQP1 channels were calculated by the method of Sogami et al. (*27*) using the following equations:

$$P_f = \left(\frac{\lambda^2}{\delta}\right)\left(\frac{kT}{h}\right)e^{(-\Delta G^{\ddagger}/RT)} \quad (1)$$

$$\Delta H^{\ddagger} = E_a - RT \quad (2)$$

$$\Delta G^{\ddagger} = \Delta H^{\ddagger} - T\Delta S^{\ddagger} \quad (3)$$

where λ is the average distance between energy minima when a molecule moves across a membrane, δ is the membrane thickness, k is Boltzmann's constant, T is the absolute temperature, h is Planck's constant, R is the ideal gas constant, E_a is the activation energy, and $\Delta G^{\ddagger}$, $\Delta H^{\ddagger}$, and $\Delta S^{\ddagger}$ are the free energy, enthalpy, and entropy of the transition state, respectively. In all calculations, δ is assumed to be 50 Å and λ is assumed to be 2.5 Å.

Immunochemical Techniques. Lysates were prepared by homogenization of eight oocytes in 160 μL of 20 mM Tris-HCl at pH 7.4, 5 mM $MgCl_2$, 5 mM NaH_2PO_4, 80 mM sucrose, 1 mM EDTA, 1 mM dithiothreitol, 1 mM PMSF, 5 μg/mL leupeptin, and 5 μg/mL pepstatin A at 4 °C with a plastic mortar and pestle. The samples were centrifuged at 125*g* for 10 min to remove the yolk proteins, and the lysate supernatant was saved for immunoblot analyses.

The lysate protein (10 μg) was resolved by SDS−polyacrylamide gel electrophoresis on 12.5% (w/v) polyacrylamide gels and were electrophoretically transferred onto polyvinylidene fluoride membranes (Immobilon) overnight at 4 °C in 0.2 M glycine, 25 mM Tris, and 20% (v/v) methanol. Membranes were incubated with shaking for 2 h at 37 °C in 10% (w/v) nonfat dry milk and 5% (v/v) goat serum in PBS (137 mM NaCl, 2.7 mM KCl, 10 mM NaH_2PO_4, and 2 mM K_2HPO_4 at pH 7.2). Membranes were washed 3 times for 5 min in PBSt [PBS at pH 7.2 and 0.01% (w/v) Tween 20]. The blot was then incubated with a 1:1000 dilution of mouse anti-FLAG antibody (Stratagene) in 1% (w/v) nonfat dry milk and 0.5% (v/v) goat serum in PBS for 1 h at 37 °C. The blots were washed with PBSt as above and were incubated with a 1:2000 dilution of horseradish peroxidase coupled-horse anti-mouse IgG (Vector Technologies) for 1 h at 37 °C. The blots were washed again with PBSt and developed with 1.25 mM luminol, 0.2 mM *p*-coumaric acid, and 0.009% (v/v) H_2O_2 in 100 mM Tris-HCl at pH 8.0. The chemiluminescent signal was detected by exposure to Fuji HR-HA 30 X-ray film.

Homology Modeling and Structural Analysis. Homology models were generated using the MOE software package (Chemical Computing Group, Quebec, Canada) as described previously (*17*). Briefly, the sequence of AtNIP6;1 was aligned with the sequence of AQP1 using the structural alignment program of MOE and the AQP1 structure (*9*). Models were constructed using the homology modeling program of MOE using the best intermediate algorithm, which generates a database of 10 individually energy-minimized models that can be separately manipulated. Models were analyzed for gross structural errors using the protein report and Ramachandran plot functions. The best model of the 10 from the database was chosen for further analysis. Molecular graphics images were generated by using the MOE or Insight II software packages (Accelerys, San Diego, CA). Pore dimensions were analyzed using HOLE (*28*).

RESULTS

Phylogeny and Homology Modeling of the Pore Regions of NIPs. The NIP family in *Arabidopsis thaliana* contains nine full-length members that fall into two phylogenetic subclasses (Figure 1B). Six NIPs (AtNIP1;1, AtNIP1;2, AtNIP2;1, AtNIP3;1, AtNIP4;1, and AtNIP4;2, designated NIP subgroup I) more closely resemble the archetype nodulin 26 in sequence, while three (AtNIP5;1, AtNIP6;1 and

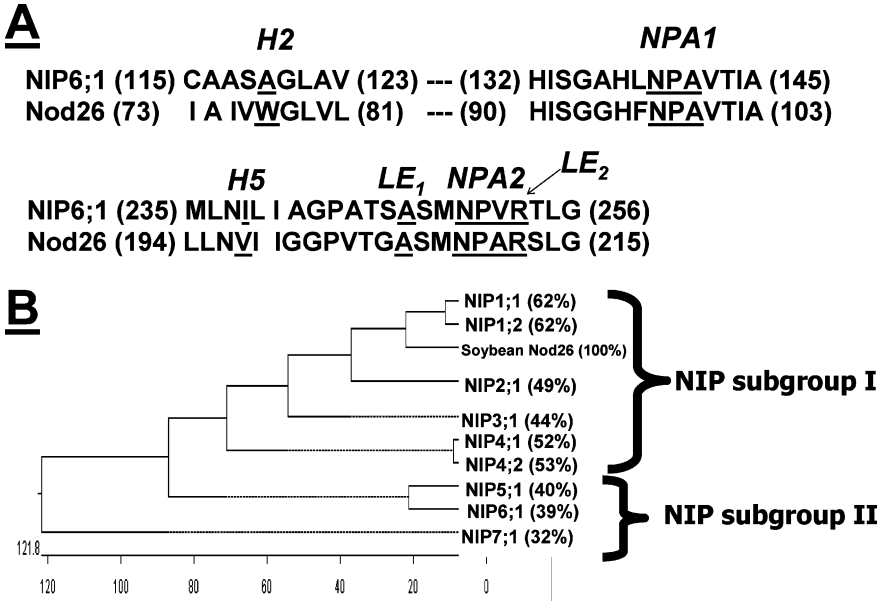

FIGURE 1: Sequence and phylogenetic analysis of members of NIP Ar/R subgroups I and II (A) Sequence alignment showing the pore determinant regions of AtNIP6;1 and soybean nodulin 26. The residues that form the ar/R filter are underlined and are indicated H2 (helix 2 position of ar/R), H5 (helix 5 position of ar/R), LE_1 (loop E 1 position of ar/R), and LE_2 (loop E 2 position of ar/R) based on the nomenclature of Wallace and Roberts (*17*). The two conserved NPA boxes, NPA 1 (N-terminal NPA motif in loop B) and NPA 2 (C-terminal NPA motif in loop E), are also indicated. Residue indices are indicated in parentheses. (B) Phylogenetic tree of the NIP subfamily from *Arabidopsis thaliana* is shown compared to the NIP family archetype soybean nodulin 26. The percent identity of each NIP family member to nodulin 26 is shown in parentheses. Braces to the right of the figure are used to indicate which NIPs are included in the NIP subgroup I (AtNIP1;1, AtNIP1;2, AtNIP2;1, AtNIP3;1, AtNIP4;1, and AtNIP4;2), and NIP subgroup II (AtNIP5;1, AtNIP6;1, and AtNIP7;1).

AtNIP7;1, designated NIP subgroup II) are more divergent (*17*). This phylogenetic divergence is apparent as well in the structure of the putative pore regions of NIP I and II subgroups. Figure 1A shows an alignment of a representative NIP I, nodulin 26, and a representative NIP II, AtNIP6;1, with the conserved sequences of the ar/R and NPA regions of the two subgroups highlighted.

The potential significance of these differences between the putative NIP I and II pore structures is apparent from a comparison of the homology models of nodulin 26 and AtNIP6;1 (Figure 2). While the overall topology of the two protein models is similar to the aquaporin I structural template, there is a clear difference in the four amino acids proposed to form the ar/R tetrad (Figure 2A). AtNIP6;1 and other NIP subgroup II members contain an unusual Ala substitution in helix 2 (H2), which is a highly conserved Trp residue in NIP subgroup I. The other ar/R residues in the AtNIP6;1/NIP subgroup II [Ile in helix 5 (H5), Ala at loop E_1 (LE_1), and Arg at loop E_2 (LE_2)] are very similar to those in nodulin 26/NIP subgroup I (Val in H5, Ala at LE_1, and Arg at LE_2) (Figures 1A and 2A). The Ala substitution at the H2 position of AtNIP6;1 creates a much wider model pore aperture at the ar/R region (5 Å) compared to nodulin 26 ar/R (3.5 Å) (Figure 2B). The smallest constriction of the AtNIP6;1 homology model pore is observed at the NPA region, which is narrower than the NPA regions of nodulin 26 model (Figure 2B), as well as the AQP1 experimental structure (*8*, *9*). This likely results from a Val substitution in the NPA2 motif of AtNIP6;1 compared to the highly conserved Ala found in nearly all MIPs (Figure 1A).

Functional Analysis of AtNIP6;1. To determine the functional consequences of the putative changes in pore architecture between AtNIP6;1 and nodulin 26, these NIPs were expressed in *Xenopus laevis* oocytes and were assayed for water as well as solute permeability. In addition, to enable analysis of the expression levels of the proteins, derivatives of each with an amino-terminal FLAG-tag sequence were analyzed (Figure 3). Western blot analysis of oocytes injected with these FLAG-tagged derivatives (AtNIP6;1F and nod26F) show equivalent expression in oocytes after 3 days of culture (Figure 3C). Analysis of the water permeability of these oocytes shows that nod26F has water-transport properties that are indistinguishable from untagged nodulin 26, with osmotic water permeabilities characteristic of those previously reported (*21*, *23*). These observations and previous reports with other MIPs (*29*) suggest that these amino-terminal tags do not affect expression, targeting, or function of these proteins.

In contrast to nodulin 26, AtNIP6;1F-expressing oocytes show no apparent facilitated water transport with P_f values indistinguishable from uninjected control oocytes (Figure 3A). However, glycerol-transport assays indicate that AtNIP6;1 is a robust glyceroporin that exhibits transport rates equivalent to soybean nodulin 26 (Figure 3B) and the bacterial glycerol permease GlpF (data not shown).

Because the predicted ar/R region of AtNIP6;1 has a larger diameter compared to nodulin 26, the ability of the two proteins to transport solutes of different sizes was tested. AtNIP6;1F and nod26F-injected ooctyes were placed in an isoosmotic solution of oocyte media containing 200 mM test solute, and the rate of oocyte swelling (dV/V_0 per unit time) resulting from an osmotic gradient associated with solute uptake was monitored. Consistent with previous analyses (*21*), nod26F readily transports formamide (van der Waals volume = 25.46 cm^3/mol), whereas the structurally related but larger urea molecule (van der Waals volume = 32.34 cm^3/mol) is excluded (Figure 4B). In contrast, the swelling rates of oocytes expressing AtNIP6;1 were identical in

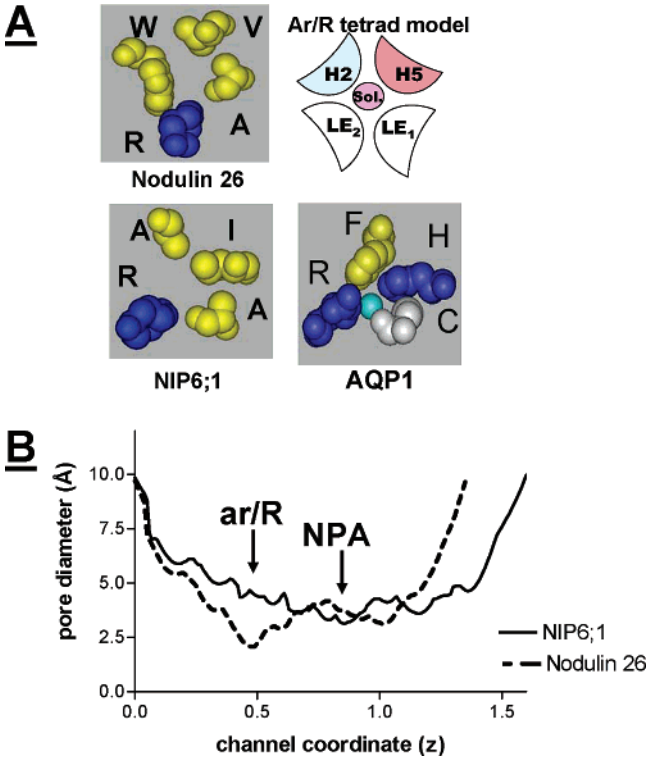

FIGURE 2: Structural comparison of the putative pore regions of NIP subgroup I and II. A homology model of AtNIP6;1 was generated with the MOE software package using the crystal structure of AQP1 [1J4N (*9*)] as a template. (A) ar/R regions of AtNIP6;1 (NIP subgroup II) and nodulin 26 (NIP subgroup I) are shown compared to the AQP1 ar/R region viewed from the extracellular side down the axis of the putative pore. Residue side chains are displayed in space-filling representation with their single-letter amino acid code and are ordered as follows from top left clockwise: helix 2, helix 5, loop E_1, and loop E_2, as shown in the ar/R tetrad model in the top right. The color scheme for residues is as follows: basic residues, blue; nonpolar residues, yellow; and small neutral hydrophilic residues, white. For a comparison, the ar/R region of AQP1 with bound water is also shown. (B) Pore diameters of nodulin 26 and AtNIP6;1 homology models were evaluated by HOLE (*28*). The pore diameters (nodulin 26, - - -; AtNIP6;1, —) are shown as a function of an arbitrary positional coordinate (channel coordinate). Positions of the ar/R and NPA motifs (determined by a comparison of traces to the trace generated with the experimental structure of AQP1; data not shown) in the two structures are indicated above the graph.

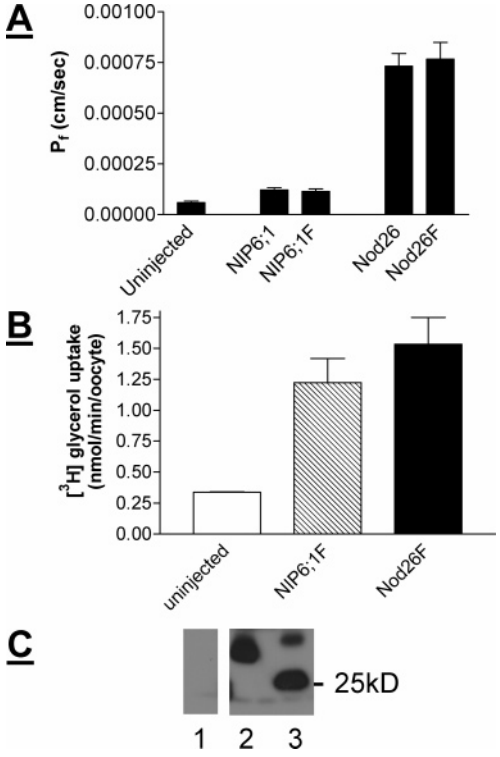

FIGURE 3: Water and glycerol permabilities of AtNIP6;1 and nodulin 26 in *Xenopus laevis* oocytes. AtNIP6;1 or nodulin 26 cRNA (46 ng) was injected into *Xenopus laevis* oocytes and was assayed for water and glycerol transport as described in the Materials and Methods. (A) Osmotic water permeability (P_f) was determined for uninjected control oocytes ($n = 31$), ooctyes expressing AtNIP6;1 ($n = 39$) and nodulin 26 ($n = 40$), or oocytes expressing AtNIP6;1F ($n = 30$) and nodulin 26F ($n = 17$), which contain an amino-terminal FLAG epitope tag. Error bars show the standard error of the mean. (B) Glycerol permeability was assessed by the uptake of ^{3}H-glycerol of uninjected oocytes or those injected with FLAG-tagged AtNIP6;1F or nodulin 26F. Error bars represent standard error of the mean (SEM) ($n = 3$). (C) Western blot of oocyte lysates (10 μg of protein/lane) resolved by SDS−PAGE on 14% (w/v) polyacrylamide gels and probed with anti-FLAG antibodies. Lane 1, uninjected control; lane 2, AtNIP6;1F; and lane 3, nodulin 26F.

formamide or urea test solutions (Figure 4A). The ability of AtNIP6;1 to transport urea was directly verified by ^{14}C-urea uptake assays (Figure 4C). While urea was readily transported by AtNIP6;1, larger uncharged solutes such as ribitol, arabitol, xylitol, and sucrose did not show measurable transport. Overall, these results support a distinct transport selectivity profile for AtNIP6;1 with extremely low water permeability but with the capability to transport some larger uncharged solutes, consistent with the larger predicted diameter of the ar/R selectivity filter from modeling results.

Substrate Selectivity of AtNIP6;1 Can Be Altered by Changing Amino Acid Residues in the ar/R Region. To investigate the functional significance of the two conserved substitutions in the putative pore region of NIP subgroup II proteins [Ala at the H2 position of the ar/R region (A119 in AtNIP6;1) and Val in the NPA2 motif (V252 in AtNIP6;1) Figure 1], these residues in AtNIP6;1 were substituted with their counterparts in the NIP subgroup I (Trp and Ala, respectively). On the basis of anti-FLAG Western blots of injected oocyte fractions, both AtNIP6;1 mutants were expressed equally well compared to nodulin 26 and AtNIP6;1 (Figure 5C). Oocytes expressing AtNIP6;1 mutants with a substitution of Ala for Val in the NPA2 region (AtNIP6;1F−V252A) showed transport properties that were indistinguishable from the wild-type AtNIP6;1 protein, exhibiting no apparent water transport, but high urea and glycerol-transport rates (Figure 4C and Figure 5). This suggests that the conserved valine substitution in the NPA region of NIP subgroup II has little effect on its transport selectivity.

In contrast, the substitution of a Trp residue for Ala at the H2 position of the ar/R tetrad of AtNIP6;1 (AtNIP6;1F−A119W) results in enhanced water-transport activity, with a P_f identical to nodulin 26 (Figure 5). Glycerol-transport assays showed that AtNIP6;1F−A119W retains the ability to facilitate glycerol transport, with rates identical to nodulin 26 and AtNIP6;1 (Figure 5B). However, analysis of the permeability of the mutant protein to the urea/formamide solute pairs (Figure 4B) shows that it becomes more restrictive, and similar to nodulin 26, selectively excludes the larger urea solute but not formamide. These data suggest

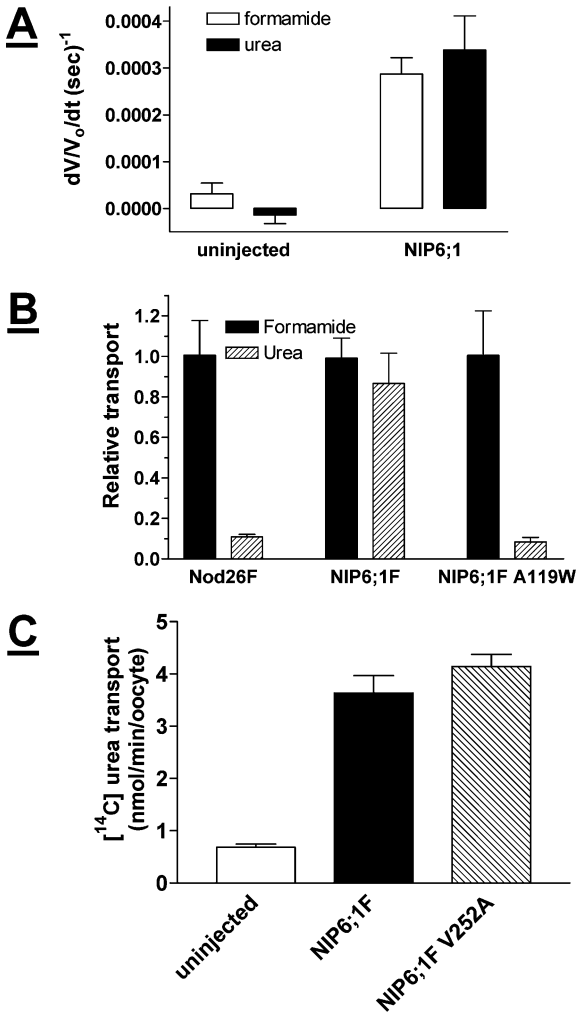

FIGURE 4: Transport selectivity of AtNIP6;1 based on solute size. (A) Ability of AtNIP6;1 to transport urea and formamide was determined by placing oocytes in an isoosmotic solution of 200 mM of each test solute and monitoring the rate of oocyte swelling (dV/V_0 per unit time) resulting from an osmotic gradient arising from solute uptake. Error bars show SEM ($n = 5$). (B) Relative transport selectivities of nodulin 26F, AtNIP6;1F, and the mutant AtNIP6;1F−A119W. The oocyte swelling rates were normalized as a fraction of the maximal rate obtained with formamide. Error bars show SEM ($n = 4-11$ oocytes). (C) Radiolabeled uptake of ^{14}C-urea was done with oocytes expressing AtNIP6;1F and AtNIP6;1F−V252A as explained in the Materials and Methods. The error bars show the SEM ($n = 3$).

that the alanine substitution within the H2 position of the ar/R filter is a critical determinant for transport substrate selectivity.

DISCUSSION

Previous investigation at the structural (*8*−*10*), computational (*12*, *14*), and biochemical (*26*, *30*) levels has implicated the ar/R region as the key selectivity filter in MIP channels. Examination of the ar/R regions of plant MIPs indicates that they are more diverse with respect to amino acid composition than their mammalian or microbial counterparts (*17*), suggesting that MIPs in plants may have different transport profiles as well as novel physiological functions. In the present study, we have found that the NIP subfamily in *Arabidopsis* contains two different subtypes of ar/R regions (NIP subgroup I and II) that display different transport selectivities.

Group I NIPs: Nodulin 26. The NIP subgroup I ar/R resembles that of soybean nodulin 26 (Figure 2), and members of this subgroup are predicted to have similar transport properties: multifunctional aquaglyceroporins with a low intrinsic water-transport rate (Table 1; *20*, *21*). This observation is supported by the two functionally characterized *Arabidopsis* members of this subgroup, AtNIP1;1 and AtNIP1;2, which have been shown to be aquaglyceroporins (*31*, *32*).

These functional properties can potentially be explained by the conserved amino acid composition of the NIP subgroup I ar/R region: Trp at H2, Val/Ile at H5, Ala at LE_1, and Arg at LE_2 (Figure 2). The Trp and Arg residues are conserved features of glyceroporins and generate the amphipathic contacts needed to interact with glycerol in the selectivity filter (*9*). Models of nodulin 26 predict that the Val and Ala side chains at H5 and LE_1 would provide a wider pore aperture compared to water-selective aquaporins that would allow the passage of glycerol. In contrast, water-selective aquaporins such as AQP1 have a highly conserved histidine at the H5 position of the ar/R (*9*, *15*, *16*). Together with the Arg at LE_2, this provides a narrower constriction and multiple hydrogen-bond contacts between the Arg and His side chains and water as it traverses the ar/R (*9*). The substitutions conserved in NIP subgroup I would generate a wider pore diameter with an ar/R region that has a lower potential to form hydrogen bonds. This may be responsible for the lower intrinsic water-transport rate observed for nodulin 26 compared with AQP1 (*20*, *21*, *26*). Consistent with this prediction, thermodynamic transition-state analysis of water transport through nodulin 26 and AQP1 proteoliposomes (Table 1) indicates a difference in the $\Delta H^{\ddagger}$ of water transport between nodulin 26 and AQP1 by about the energy of a hydrogen bond (4−8 kJ/mol). These data are in agreement with the substitution of a Val for His in nodulin 26, which would eliminate a potential hydrogen-bond donor in the ar/R region.

Group II NIPs: AtNIP6;1. While the NIP subgroup II ar/R shares many of the same properties as the NIP subgroup I, it is distinguished by a single nonconservative amino acid substitution of Ala at position H2 for the Trp residue that is conserved in NIP subgroup I and virtually all other known glycerol permeases. On the basis of modeling, using the AQP1 template, the structural consequence of this substitution is predicted to be an increase in the diameter of the NIP subgroup II ar/R region (5 Å for NIP subgroup II and 3.5 Å for NIP subgroup I based on HOLE measurements) and a decrease in the hydrophobicity of the ar/R region.

AtNIP6;1 also contains an Ala to Val substitution in the second conserved Asn−Pro−Ala (NPA) motif found in loop E. Similar substitutions have been observed both in the ar/R and NPA regions in other type-II *Arabidopsis* NIPs [e.g., AtNIP5;1 (*17*)], as well as in NIPs isolated from *Atriplex nummularia* (*33*), suggesting that these features might be typical of NIP subgroup II. Structural analysis of the pore regions of the homology models suggest that, in contrast to most known MIP structures (*8*−*10*), the narrowest constriction of the AtNIP6;1 pore seems to be at the NPA region. This structural feature probably results from the substitution of Val for Ala at the C-terminal NPA box in AtNIP6;1.

Functional analysis of AtNIP6;1 as well as soybean nodulin 26 indicates that both NIPs are highly permeable to

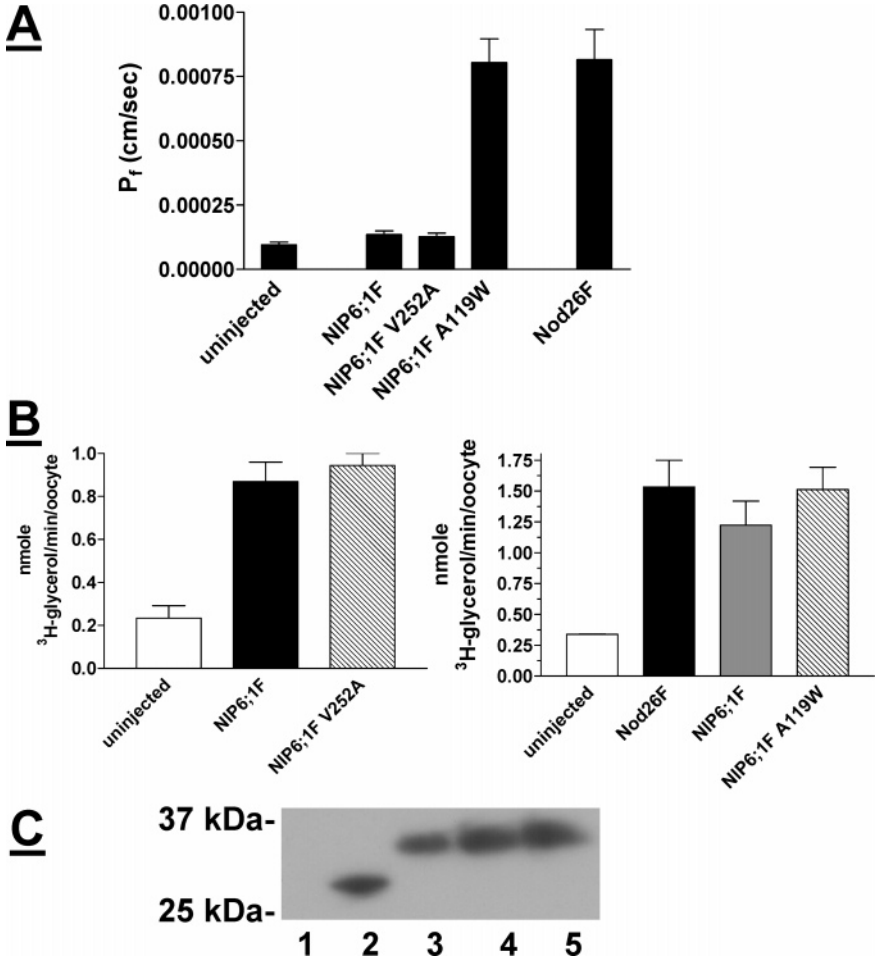

FIGURE 5: Transport properties of AtNIP6;1 with site-specific substitutions in pore-determinant regions. FLAG-tagged AtNIP6;1 mutants with substitutions in the NPA2 region (NIP6;1F−V252A) or the H2 position of the ar/R region (NIP6;1F−A119W) were expressed in *Xenopus* oocytes and assayed for glycerol and water transport as described in Figure 3. (A) Osmotic water permeability (P_f) was determined for uninjected control oocytes ($n = 20$) or ooctyes expressing AtNIP6;1F ($n = 19$), AtNIP6;1F−V252A ($n = 20$), AtNIP6;1F−A119W ($n = 7$), and nodulin 26F ($n = 11$). Error bars show the SEM. (B) To the left, glycerol permeability was assessed by the uptake of ^{3}H-glycerol by uninjected oocytes or those injected with AtNIP6;1F or AtNIP6;1F−V252A. Error bars represent SEM ($n = 3$). To the right, the glycerol permeabilities of Nod26F, NIP6;1F, and NIP6;1F−A119W are compared. Error bars represent SEM ($n = 3$). (C) Western blot of oocyte lysates (10 μg of protein/lane) resolved on 12.5% polyacrylamide gels and probed with anti-FLAG antibody. Lane 1, uninjected; lane 2, Nod26F; lane 3, NIP6;1F; lane 4, NIP6;1F−V252A; and lane 5, NIP6;1F−A119W.

Table 1: Transition-State Analysis of Group I NIP Water Transport

membrane[a]	E_a (kJ/mol)[b]	$\Delta H^{\ddagger}$ (kJ/mol)[c]	$\Delta S^{\ddagger}$ (e.u.)	p_f[d] (cm^3/s)
control liposomes	61.9	59.4	24.1	
AQP1 proteoliposome	9.20	6.65	−19.6	11.4×10^{-14}
nodulin 26 proteoliposome	17.0	14.6	−17.5	0.38×10^{-14}

[a] Reconstitution of proteoliposomes was done as in ref *20*. The data for AQP1 is taken from ref *39*. [b] Activation energy as calculated from Arrhenius plots as in ref *20*. [c] ΔH and ΔS of the transition state for water transport as calculated using the equations derived in ref *27* (see the Materials and Methods). [d] The nodulin 26 unitary water permeability (p_f) per protein monomer was determined as described previously (*20*). The data for AQP1 are from ref *40*.

glycerol as well as formamide and transport these solutes at similar rates. However, AtNIP6;1 differs from nodulin 26 because it exhibits no measurable water permeability and shows the ability to flux larger solutes such as urea. Consistent with this observation, urea transport has been found to be associated with zucchini NIP1 (*34*), which has a sequence characteristic of the NIP subgroup II class. These results indicate that NIP subgroups I and II are functionally as well as structurally distinct and probably play different roles in plant-membrane transport and water balance. The NIP subgroup II proteins also represent a novel group of plant MIPs that are glycerol/solute-specific and have very low water permeability, similar to bacterial glycerol facilitators such as GlpF (*30*, *35*).

To investigate which features of the NIP subgroup II pore are responsible for its unique transport properties, site-directed mutagenesis of the two unusual conserved residues (i.e., Val in the second NPA box and Ala in the H2 position of the ar/R) was done. Surprisingly, the substitution of an Ala for Val 252 resulted in an AtNIP6;1 protein that was functionally identical to the wild-type protein with respect to transport rates and selectivities with all tested solutes. This result suggests that the substitution of a bulkier Val for Ala at this position is not important for determining the transport profile of AtNIP6;1 with respect to the assayed substrates.

In contrast, substitution of a Trp for Ala at the H2 position of the putative AtNIP6;1 ar/R region (AtNIP6;1−A119W) had a dual effect on activity. The A119W mutant acquired the ability to facilitate water transport with a P_f identical to type-I NIPs such as nodulin 26. Additionally, the substitution

of the bulkier Trp residues provides a greater size restriction on transport, resulting in the exclusion of urea, again similar to the type-I NIPs.

The extremely low water permeability of AtNIP6;1 is perplexing considering that the modeled pore is 5 Å in diameter, large enough to accommodate approximately two water molecules. Furthermore, the ar/R region contains all of the putative hydrogen-bond donors and acceptors (the backbone carbonyl of Ala in LE_1 and the guanido group of Arg at LE_2 are conserved in both nodulin 26 and AtNIP6;1) that are present in the NIP subgroup I members, suggesting that AtNIP6;1 should be capable of transporting water at a similar rate to nodulin 26. The reason for this low water permeability remains unknown but could conceivably arise from several different sources. A gating mechanism has been proposed to account for the low water permeability of the bacterial glycerol facilitator GlpF (*12*), in which the Trp residue at helix 2 of the ar/R moves when it comes into contact with glycerol to allow the solute to pass through the pore. In this scheme, water cannot open the gate, but it is cotransported with glycerol, accounting for the low but measurable water permeability of GlpF.

Alternatively, the glycerol-transport function of the yeast aquaglyceroporin Fps1 has been shown to be gated by hydrophilic cytosolic domains at the N and C termini (*36*, *37*). Group II NIPs such as AtNIP5;1 and NIP6;1 have unique extended amino-terminal domains (*17*) that could potentially have a similar function. A final hypothesis based on thermodynamic considerations is that AtNIP6;1 may not be able to properly organize water at the ar/R region because of the larger size of this region. Sui et al. (*9*) proposed that, in the AQP1 structure, the hydrophobic Phe residue at H2 position of the ar/R filter is positioned such that it orients water to form maximal hydrogen-bonding overlap with the hydrogen-bond donors and acceptors in the ar/R region. Aquaporin-mediated water transport shows a strong entropic component (*27*), with a highly negative $\Delta S^{\ddagger}$ and a low positive $\Delta H^{\ddagger}$ (e.g., see Table 1), suggesting that organization in the transport process is essential. Indeed, MIPs such as AQP1 with a high transport rate for water have smaller ar/R regions that are highly hydrophilic.

TIPs and NIPs: The Importance of the H2 Position of the ar/R. The present results suggest that the H2 position of the ar/R region is the major site of transport selectivity in the NIP subfamily. This position may also help determine the selectivity of other plant MIPs, including some members of the TIP subclass of plant aquaporins. A comparison of the ar/R residues of the NIP and TIP subclasses from modeling results (*17*) show that the ar/R composition is similar, with the principal difference occurring at the H2 position (Figure 6). The substitution of a highly conserved His residue at the H2 position of TIPs would increase the hydrophilicity and hydrogen-bond-forming potential of the ar/R, similar to AQP1 and other water-selective aquaporins (*9*, *10*, *15*). In support of this, site-directed mutagenesis of the conserved Trp at H2 of NIP subgroup I proteins with a His results in the loss in the ability to transport glycerol, while water transport is largely unaffected (Figure 6). It should be noted that some members of the TIP family have been shown to transport other solutes including urea (*34*, *38*), and thus, other properties of the TIP pore distinct from the NIP pore lead to this altered selectivity. Nevertheless, it is clear that selectivity for water and glycerol of three separate groups of plant MIPs (NIP I, NIP II, and TIPs) may be largely determined by a single residue in helix 2 with His for TIP aquaporins, Trp for NIP I aquaglyceroporins, and Ala for NIP II glyceroporins that do not transport water.

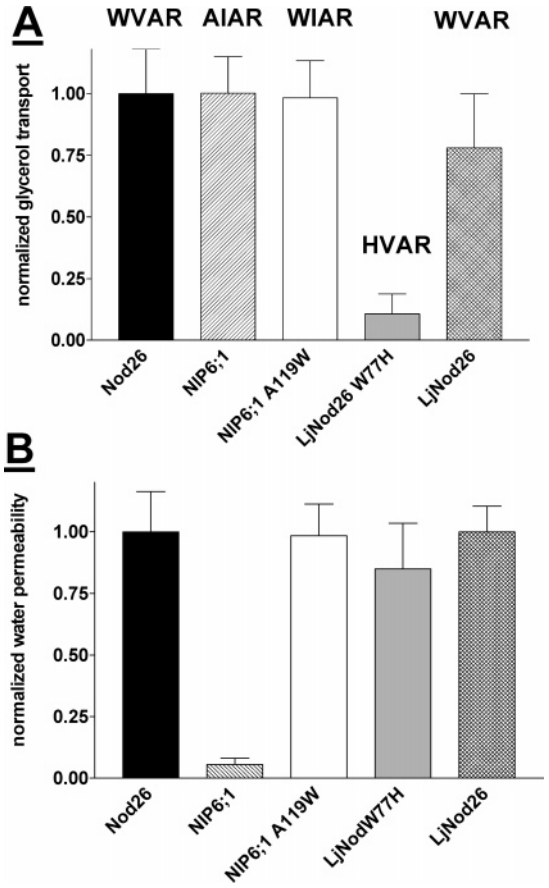

FIGURE 6: Comparison of NIP and TIP ar/R substitutions at H2 on water and glycerol transport. Shown are the transport characteristics of NIPs with ar/R regions with substitutions at the H2 position. The data are corrected for basal water and glycerol transport (i.e., uninjected oocytes) and are normalized to nodulin 26 transport. Nod26, soybean nodulin 26; NIP6;1, AtNIP6;1; NIP6;1−A119W, AtNIP6;1 with a Trp substitution at the H2 position; LjNod26−W77H; wild-type LjNod26 with a substitution of a His for Trp at H2. LjNod 26 represents the orthologue of nodulin 26 from *Lotus japonicus* (*26*). (A) Normalized glycerol transport. (B) Normalized osmotic water permeability. The ar/R compositions of each test protein is listed over the bars in A in the order of H2, H5, LE_1, and LE_2. Error bars show SEM.

ACKNOWLEDGMENT

We thank Dr. James Guenther for critical comments on the manuscript prior to submission.

REFERENCES

1. Johanson, U., Karlsson, M., Johansson, I., Gustavsson, S., Sjovall, S., Fraysse, L., Weig, A. R., and Kjellbom, P. (2001) The complete set of genes encoding major intrinsic proteins in *Arabidopsis* provides a framework for a new nomenclature for major intrinsic proteins in plants, *Plant Physiol. 126*, 1358−1369.
2. Quigley, F., Rosenberg, J. M., Shachar-Hill, Y., and Bohnert, H. J. (2002) From genome to function: The *Arabidopsis* aquaporins, *Genome Biol. 3*, 1−17.
3. Chaumont, F., Barrieu, F., Herman, E. M., and Chrispeels, M. J. (1998) Characterization of a maize tonoplast aquaporin expressed in zones of cell division and elongation, *Plant Physiol. 117*, 1143−1152.

4. Martre, P., Morillon, R., Barrieu, F., North, G. B., Nobel, P. S., and Chrispeels, M. J. (2002) Plasma membrane aquaporins play a significant role during recovery from water deficit, *Plant Physiol. 130*, 2101−2110.
5. Tournaire-Roux, C., Sutka, M., Javot, H., Gout, E., Gerbeau, P., Luu, D. T., Bligny, R., and Maurel, C. (2003) Cytosolic pH regulates root water transport during anoxic stress through gating of aquaporins, *Nature 425*, 393−397.
6. Tyerman, S. D., Niemietz, C. M., and Bramley, H. (2002) Plant aquaporins: Multifunctional water and solute channels with expanding roles, *Plant Cell Environ. 25*, 173−194.
7. Maurel, C., Javot, H., Lauvergeat, V., Gerbeau, P., Tournaire, C., Santoni, V., and Heyes, J. (2002), Molecular physiology of aquaporins in plants, *Int. Rev. Cytol. 215*, 105−148.
8. Fu, D., Libson, A., Miercke, L. J., Weitzman, C., Nollert, P., Krucinski, J., and Stroud, R. M. (2000), Structure of a glycerol-conducting channel and the basis for its selectivity, *Science 290*, 481−486.
9. Sui, H., Han, B. G., Lee, J. K., Walian, P., and Jap, B. K. (2001) Structural basis of water-specific transport through the AQP1 water channel, *Nature 414*, 872−878.
10. Harries, W. E., Akhavan, D., Miercke, L. J., Khademi, S., and Stroud, R. M. (2004) The channel architecture of aquaporin 0 at a 2.2 Å resolution, *Proc. Natl. Acad. Sci. U.S.A. 101*, 14045−14050.
11. Jung, J. S., Preston, G. M., Smith, B. L., Guggino, W. B., and Agre, P. (1994) Molecular structure of the water channel through aquaporin CHIP. The hourglass model, *J. Biol. Chem. 269*, 14, 648−14654.
12. Tajkhorshid, E., Nollert, P., Jensen, M. O., Miercke, L. J., O'Connell, J., Stroud, R. M., and Schulten, K. (2002) Control of the selectivity of the aquaporin water channel family by global orientational tuning, *Science 296*, 525−530.
13. Ilan, B., Tajkhorshid, E., Schulten, K., and Voth, G. A. (2004) The mechanism of proton exclusion in aquaporin channels, *Proteins 55*, 223−228.
14. de Groot, B. L., and Grubmuller, H. (2001) Water permeation across biological membranes: Mechanism and dynamics of aquaporin-1 and GlpF, *Science 294*, 2353−2357.
15. Thomas, D., Bron, P., Ranchy, G., Duchesne, L., Cavalier, A., Rolland, J. P., Raguenes-Nicol, C., Hubert, J. F., Haase, W., and Delamarche, C. (2002) Aquaglyceroporins, one channel for two molecules, *Biochim. Biophys. Acta 1555*, 181−186.
16. Stroud, R. M., Savage, D., Miercke, L. J., Lee, J. K., Khademi, S., and Harries, W. (2003) Selectivity and conductance among the glycerol and water conducting aquaporin family of channels, *FEBS Lett. 555*, 79−84.
17. Wallace, I. S., and Roberts, D. M. (2004) Homology modeling of representative subfamilies of *Arabidopsis* major intrinsic proteins. Classification based on the aromatic/arginine selectivity filter, *Plant Physiol. 135*, 1059−1068.
18. Weaver, C. D., Crombie, B., Stacey, G., and Roberts, D. M. (1991) Calcium-dependent phosphorylation of symbiosome membrane proteins from nitrogen-fixing soybean nodules. Evidence for phosphorylation of nodulin 26, *Plant Physiol. 95*, 222−227.
19. Fortin, M. G., Morrison, N. A., and Verma, D. P. (1987) Nodulin-26, a peribacteroid membrane nodulin is expressed independently of the development of the peribacteroid compartment, *Nucleic Acids Res. 15*, 813−824.
20. Dean, R. M., Rivers, R. L., Zeidel, M. L., and Roberts, D. M. (1999) Purification and functional reconstitution of soybean nodulin 26. An aquaporin with water and glycerol transport properties, *Biochemistry 38*, 347−353.
21. Rivers, R. L., Dean, R. M., Chandy, G., Hall, J. E., Roberts, D. M., and Zeidel, M. L. (1997) Functional analysis of nodulin 26, an aquaporin in soybean root nodule symbiosomes, *J. Biol. Chem. 272*, 16256−16261.
22. Weaver, C. D., and Roberts, D. M. (1992) Determination of the site of phosphorylation of nodulin 26 by the calcium-dependent protein kinase from soybean nodules, *Biochemistry 31*, 8954−8959.
23. Guenther, J. F., Chanmanivone, N., Galetovic, M. P., Wallace, I. S., Cobb, J. A., and Roberts, D. M. (2003) Phosphorylation of soybean nodulin 26 on serine 262 enhances water permeability and is regulated developmentally and by osmotic signals, *Plant Cell 15*, 981−991.
24. Preston, G. M., Carroll, T. P., Guggino, W. B., and Agre, P. (1992) Appearance of water channels in *Xenopus* oocytes expressing red cell CHIP28 protein, *Science 256*, 385−387.
25. Guenther, J. F., and Roberts, D. M (2000) Water-selective and multifunctional aquaporins from *Lotus japonicus* nodules, *Planta 210*, 741−748.
26. Wallace, I. S., Wills, D. M., Guenther, J. F., and Roberts, D. M. (2002) Functional selectivity for glycerol of the nodulin 26 subfamily of plant membrane intrinsic proteins, *FEBS Lett. 523*, 109−112.
27. Sogami, M., Era, S., Murakami, M., Seo, Y., Watari, H., and Uyesaka, N. (2001) Application of the transition state theory to water transport across cell membranes, *Biochim. Biophys. Acta 1511*, 42−48.
28. Smart, O. S., Goodfellow, J. M., and Wallace, B. A. (1993) The pore dimensions of gramicidin A, *Biophys. J. 65*, 2455−2460.
29. Yang, B., and Verkman, A. S. (1997) Water and glycerol permeabilities of aquaporins 1−5 and MIP determined quantitatively by expression of epitope-tagged constructs in *Xenopus* oocytes, *J. Biol. Chem. 272*, 16140−16146.
30. Borgnia, M. J., and Agre, P. (2001) Reconstitution and functional comparison of purified GlpF and AqpZ, the glycerol and water channels from *Escherichia coli*, *Proc. Natl. Acad. Sci. U.S.A. 98*, 2888−2893.
31. Weig, A., Deswarte, C., and Chrispeels, M. J. (1997) The major intrinsic protein family of *Arabidopsis* has 23 members that form three distinct groups with functional aquaporins in each group, *Plant Physiol. 114*, 1347−1357.
32. Weig, A. R., and Jakob, C. (2000) Functional identification of the glycerol permease activity of *Arabidopsis thaliana* NLM1 and NLM2 proteins by heterologous expression in *Saccharomyces cerevisiae*, *FEBS Lett. 481*, 293−298.
33. Cabello-Hurtado, F., and Ramos, J. (2004) Isolation and functional analysis of the glycerol permease activity of two new nodulin-like intrinsic proteins from salt stressed roots of the halophyte *Atriplex nummularia*, *FEBS Lett. 166*, 633−640.
34. Maurel, C., Reizer, J., Schroeder, J. I., Chrispeels, M. J., and Saier, M. H. (1994) Functional characterization of the *Escherichia coli* glycerol facilitator, GlpF, in *Xenopus* oocytes, *J. Biol. Chem. 269*, 11869−11872.
35. Klebl, F., Wolf, M., and Sauer, N. (2003) A defect in the yeast plasma membrane urea transporter Dur3p is complemented by CpNIP1, a Nod26-like protein from zucchini (*Cucurbita pepo* L.) and by *Arabidopsis thaliana* δ-TIP or γ-TIP, *FEBS Lett. 547*, 69−74.
36. Tamas, M. J., Karlgren, S., Bill, R. M., Hedfalk, K., Allegri, L., Ferreira, M., Thevelein, J. M., Rydstrom, J., Mullins, J. G., and Hohmann, S. (2003) A short regulatory domain restricts glycerol transport through yeast Fps1p, *J. Biol. Chem. 278*, 6337−6345.
37. Hedfalk, K., Bill, R. M., Mullins, J. G., Karlgren, S., Filipsson, C., Bergstrom, J., Tamas, M. J., Rydstrom, J., and Hohmann, S. (2003) A regulatory domain in the C-terminal extension of the yeast glycerol channel Fps1p, *J. Biol. Chem. 279*, 14954−14960.
38. Liu, L.-H., Ludewig, U., Gassert, B., Frommer, W. B., and von Wiren, N. (2003) Urea transport by nitrogen-regulated tonoplast intrinsic proteins in *Arabidopis*, *Plant Physiol. 133*, 1220−1228.
39. van Hoek, A. N., and Verkman, A. S. (1992) Functional reconstitution of the isolated erythrocyte water channel CHIP28, *J. Biol. Chem. 267*, 18267−18269.
40. Zeidel, M. L., Ambudkar, S. V., Smith, B. L., and Agre, P. (1992) Reconstitution of functional water channels in liposomes containing purified red cell CHIP28 protein, *Biochemistry 31*, 7436−7440.

BI0511888